Chapter 3

Sample Preparation and Characterization

This chapter summarizes the experimental methods used to prepare and characterize the material investigated in this work. In the first section the measurement techniques applied to study the material properties are discussed. The second part describes the basics of the deposition techniques, namely plasma enhanced chemical vapor deposition (PECVD) and hot wire chemical vapor deposition (HWCVD). As for different characterization methods different substrates and device structures are needed, the last section will provide an overview of the particular sample preparations and treatments.

3.1 Characterization Methods

The aim of this section is describe the potential, but also the limitations of the individual techniques used for the material characterization. In this study, Raman spectroscopy was used to determine the crystallinity of the material, paramagnetic states were studied by electron spin resonance (ESR) and transport properties were investigated using conductivity measurements and transient photocurrent experiments (TOF).

3.1.1 Raman Spectroscopy

Raman spectroscopy can provide detailed information about the vibrational properties of solids, liquids, and gases. A detailed description of the underlying physics can be found in the literature [105, 106]. Reviews of the application to μc-Si:H can be found in [107, 108] and a detailed description of the setup used in this work

in [109, 52]. Here Raman spectroscopy has been used to determine the crystalline volume content of the μc-Si:H material.

As described in section 2.1 μc-Si:H is a phase mixture of crystalline and amorphous material. A typical Raman spectrum, as shown in Fig. 3.1, is a convolution of a crystalline and an amorphous spectrum. Spectra of crystalline silicon are dominated by a peak at 520 cm^{-1} attributed to the transversal optical (TO) phonon. Due to the finite grain size and internal stress in μc-Si:H this peak shifts to lower values (usually found at 518 cm^{-1}) and the peak width increases [110, 107]. As a result of the absence of long range translation symmetry in a-Si:H, the quantum number $\vec{k}$ is no longer well-defined and the excitation of a phonon is possible without restriction of $\vec{k}$ preservation. In a-Si:H, one therefore observes a broad intensity distribution of the TO-phonon at 480 cm^{-1}. Besides these two peaks a third peak at around 492 cm^{-1} is often observed in μc-Si:H Raman spectra. This peak is a result of stacking faults in the crystalline phase, also referred to as wurtzite peak [111].

To account for the asymmetry, the crystalline peak was fitted by two Gaussian lines centered at 518 cm^{-1} and 505 cm^{-1}. As a measure of the crystallinity, the Raman intensity ratio I_C^{RS} was used, defined as

$$I_C^{RS} = \frac{I_{518} + I_{505}}{I_{518} + I_{505} + I_{480}}. \tag{3.1}$$

For a given sample, I_C^{RS} was determined by de-convoluting the spectra into three contributions at wave numbers of 518, 505 and 480 cm^{-1}. Although I_C^{RS} is related to the volume content of crystalline and disordered phase this evaluation must be used carefully. The Raman cross sections for crystalline and amorphous silicon are different and additionally they depend on the wavelength of the incident laser light. Measured by Tsu et al. [112], the cross section ratio at $\lambda = 496.5$ nm is σ_c/σ_a=0.88. Additionally, grain boundaries may lead to a signal at 480 cm^{-1} [113]. For these reasons I_C^{RS} can be considered as a lower limit of the crystalline volume content.

Information about the distribution of the crystalline volume fraction in the growth direction can be obtained by using different excitation wavelengths λ. In this work laser wavelengths of 488 nm and 647 nm were used, that corresponds to an information depth[1] of 150 nm and 800 nm, respectively.

The validity of the determination of the crystallinity by Raman spectroscopy used in this work is still under discussion. While Ossadnik et al. [114] found no correlation between the Raman intensity ratio and the crystalline volume fraction obtained from X-ray diffraction measurements, recent work in the Juelich group

---

[1]The information depth is defined as half of the absorption depth (depth where the signal is attenuated to a fraction of $1/e$).
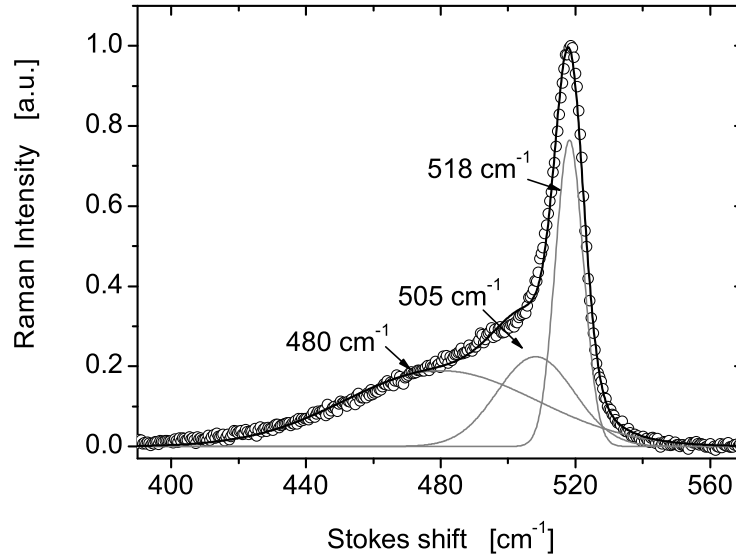
Figure 3.1: *Typical Raman spectrum of a µc-Si:H film.*

shows a clear correlation between I_C^{RS}, X-ray diffraction and TEM [115, 116]. However, there is broad agreement that the crystallinity is underestimated by the Raman intensity ratio.

3.1.2 Electron Spin Resonance (ESR)

Since the first spectrum recorded in 1945 [117], electron spin resonance (ESR)[2] has developed into a powerful spectroscopic technique used in many areas of modern physics, chemistry and biology. The subject matter of ESR is the interaction of electrons with magnetic fields and with each other. In this section the physical principles of ESR will be briefly discussed, followed by a brief description of the actual measurement.

3.1.2.1 Spin Hamiltonian

For a system containing only one unpaired electron spins (S=1/2) the Hamilton operator can be written as

$$\mathcal{H} = g_0 \mu_B B_0 \mathbf{S} + \mu_B B_0 [\Delta g] \mathbf{S}. \tag{3.2}$$

where g_0 is the electronic g-value for a free electron (≈ 2.0023), μ_B the Bohr magneton, B_0 is the flux density, $[\Delta g]$ is the interaction tensor of the spin orbit

---

[2]In the literature also referred to as Electron Paramagnetic Resonance (EPR)

coupling, and **S** the spin operator [118]. For the following discussion, terms due to hyperfine interaction, the interaction with the nuclei spin, and the spin-spin interaction are neglected because they have no resolvable contribution to the spectra measured in this work.

In Eq. 3.2 the second term describes the coupling of the electron spin with the magnetic moment of the orbital angular moment **L**, whereas the tensor quantity $[\Delta g]$ describes the deviation of the g-value from that of the free electron g_0. In covalent semiconductors, where the electronic eigenstates are usually described in terms of s- and p-state wavefunctions, **L**, whose eigenstates are degenerate, has a zero expectation value if the crystal field interaction greatly exceeds the Zeeman term [24]. This effect is known as quenching of the orbital angular momentum by the crystal field. In this special case the second term in Eq. 3.2 becomes zero.

However, due to the interaction with a magnetic field the degeneracy of the eigenstates of **L** is lifted and the quenching is partly removed. For an unpaired electron in the ground state, the elements of the g-tensor g_{ij} in the second term of Eq. 3.2 are given by [118]

$$g_{ij} = -2\lambda \sum_{n(\neq 0)} \frac{< \Psi_0|L_i|\Psi_n >< \Psi_n|L_j|\Psi_0 >}{E_n - E_0} \qquad (3.3)$$

where λ is the spin orbit coupling parameter. The index n counts all other orbitals Ψ_n, E_0 denotes the energy of the ground state and E_n the energy of the state Ψ_n. The g-value is therefore an important quantity in ESR measurements and serves to distinguish and identify electronic states. However, in disordered or powdered material the angular dependence is masked as all orientations can be observed at the same time. The obtained spectra are called "powder spectrum".

3.1.2.2   Lineshape and Linewidth

Besides the g-value, the shape and the width of the resonance line contains a number of information about the spin system [119, 118]. It is important to note that in ESR one talks about the peak-to-peak width, which is defined as the width between the maximum and minimum of the derivative of the absorption line. Depending on the specific lineshape of the curve this value differs by a numerical factor from the linewidth at half maximum (FWHM) typically used in other spectroscopy methods.

In general one distinguishes between two different mechanisms broadening the resonance line, first the "homogeneous" broadening which is caused by the relaxation of the excited spin state and second the inhomogeneous broadening as a result of an unresolved overlap of different ESR lines.

Homogeneous Broadening

Because of the finite lifetime of an electron in the excited state, the uncertainty principle leads to a finite so called "natural linewidth". While an excited electron is re-enters its ground state its energy will be transferred to the surrounding lattice. Within a time T_1 the spin-lattice relaxation restores the system into its the equilibrium state. In addition, there is an interaction of the spins with each other. The time constant of this spin-spin relaxation process is typically denoted T_2. From the spin-lattice and spin-spin relaxation the lineshape is of the form of a Lorentzian [118].

Inhomogeneous Broadening

Differences from the Lorentzian line shape discussed above can arise from g-value anisotropy or an unresolved hyperfine interaction. Additionally broadening can also result from structural disorder. In this case the overall resonance line consists of a number of narrower individual lines, that are a result of the so-called spin packets. Each spin packet can be seen as an individual system of spins, having the same Lamor frequency ω_i around "their" magnetic field vectors B_i. In general B_i is given by the sum of the externally applied field B_0 and the local field B_i^{loc}. Due to inhomogeneities, like crystal irregularities, magnetic field inhomogeneities, or dipolar interaction between unlike spins, the local field B_i^{loc} differs for spins belonging to different spin packets. The observed line shape is therefore a contribution of several Lorentzian signals arising from different spin packets. For disordered semiconductors like amorphous and microcrystalline silicon both, the energetic position as well as the local environment of the spins may not be identical, which leads to numerous slightly different g-values. Both effects are expected to be statistically distributed and thus the resulting line shape of the convolution of the homogeneous lines is of the form of a Gaussian.

3.1.2.3   Experimental Setup

ESR has been measured using a commercial X-band spectrometer (BRUKER ESP 380E). A reflex klystron working at a frequency of around 9.3 GHz with a maximum power output of about 200 mW was used as the microwave source. During the measurement the microwave frequency was kept constant while the resonance conditions were reached by scanning the magnetic field B_0. The ESR signal was recorded using phase sensitive detection so that the measured signal intensity is proportional to the first derivative of the absorption signal. The area under the absorption curve, which is proportional to the spin density N_S, was obtained by double integrating the measured signal, numerically. For a quantitative analysis

of the ESR spectra (calculation of the g-value and the spin density N_S) the ESR signal was compared to that of a sample of un-hydrogenated sputtered amorphous silicon, which was calibrated to a standard of Picein and DPPH [120]. For temperature dependent measurements a He gas flow cryostat (Oxford ESR 900) was used. To avoid condensation of water at the walls the cavity was purged with dry nitrogen.

ESR measurements were performed in a temperature range between 4.5 K and 300 K using a modulation frequency of 100 kHz and a modulation amplitude of 2 G. The microwave power could be attenuated in the range between 200 mW - 0.2 μW and was usually set such that saturation effects did not occur. Details of the sample handling and the preparation can be found in section 3.3.1.

3.1.3 Electrical Conductivity

Conductivity measurements were performed on specimens deposited on roughened borosilicate glass prepared in the same run as the samples prepared for ESR measurements. As contacts, coplanar silver pads were evaporated under high vacuum conditions having a thickness of 700 nm, an electrode spacing b=0.5 mm, and a width l=4 mm. In order to avoid errors due to surface coverage all measurements were performed under high vacuum ($p < 0.01$ Pa) conditions after an annealing step of 30 min at 450 K (compare section 6 and 6.3). To ensure that the determined conductivity is voltage independent (ohmic contacts), I-V curves have been measured between $V = \pm 100$ V.

Having determined the current I for an applied voltage V (usually set to V=100 V) the specific dark conductivity σ_D is given by

$$\sigma_D = \frac{b \cdot I}{l \cdot d \cdot V} \tag{3.4}$$

where d is the film thickness and l, b are determined by the contact geometry (see above).

Temperature dependent measurements were performed between 100 K and 450 K using a nitrogen cooled continuous flow cold finger cryostat.

3.1.4 Transient Photocurrent Measurements (TOF)

The time-of-flight (TOF) technique was first described by J.R. Haynes and W. Shockley in 1951 [121] and was further improved by R. Lawrence and A.F. Ribson in 1952 [122]. The first application to an amorphous material (a-Se) was first done by W. Spear in 1957 [123, 124, 125] and since then it has widely been used to obtain valuable information on transport processes in a wide range of low mobility amorphous and crystalline solids.
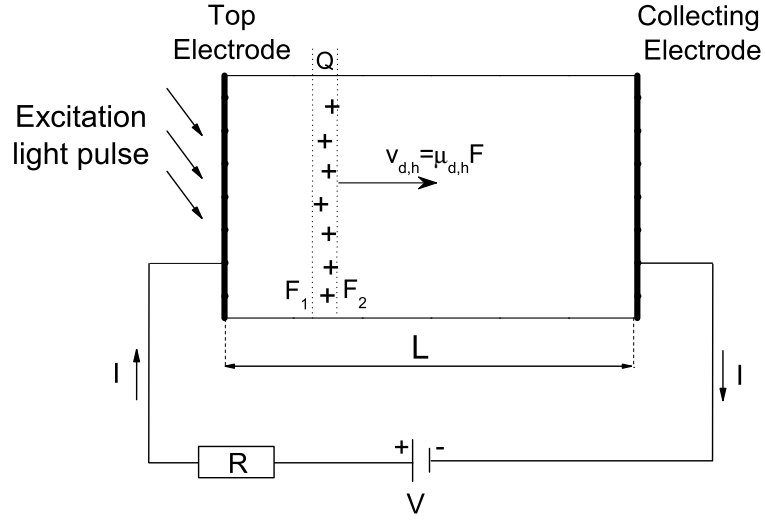
Figure 3.2: *Schematic view of a time-of-flight experiment.*

3.1.4.1 Basic Features of the Time-of-Flight Technique

The aim of the experiment is to measure the time required for a charge carrier packet to drift from one side of the sample to the other under the influence of an applied electric field. The simplest embodiment of a time-of-flight experiment is illustrated in Fig. 3.2. The material of interest is sandwiched between two contacts; one, preferably both are semitransparent. Electron-hole pairs are injected on one side of the dielectric at a time $t = 0$ using a short flash of strongly-absorbed light. Depending on the direction of the applied electric field $F = V/L$, where V is the applied voltage and L the thickness of the sample, either the electrons or the holes are drawn across the material with a drift velocity of

$$\mathrm{v}_d = \mu_d F. \tag{3.5}$$

This drifting charge carrier sheet will modify the applied field F. Simple electrostatic considerations show that the electric fields F_1 and F_2 indicated in Fig. 3.2 are given by

$$F_1(t) = F - \frac{q}{\varepsilon\varepsilon_0}\left(1 - \frac{\mathrm{v}_d t}{L}\right) \tag{3.6}$$

$$F_2(t) = F + \frac{q}{\varepsilon\varepsilon_0}\left(\frac{\mathrm{v}_d t}{L}\right) \tag{3.7}$$

where q is the charge carrier density, ε is the dielectric constant of the material, ε_0 the dielectric constant of the vacuum, and t the time [125, 126, 127]. These time dependent electric fields F_1 and F_2 will in turn induce a redistribution of the

25

charge at the electrodes. The current induced by this redistribution is called displacement current. As the current has to be the same everywhere in the circuit, the displacement current inside the sample has to be matched by an identical current in the external circuit. The drift motion of the charge carrier packet can therefore be detected by measuring the current induced in the external circuit. This current

$$I = \frac{q \mathrm{v}_d}{L} \qquad (3.8)$$

is determined by the product of the injected charge q with its average drift velocity v_d normalized to the sample thickness L. While they are in motion the drifting charge carriers generate a displacement current which terminates when reaching the back contact. From the arrival time t_τ an average drift mobility μ_d

$$\mu_d = \frac{L^2}{V t_\tau} = \frac{L}{F t_\tau} \qquad (3.9)$$

can be determined.

Two facts are important to note at this point: (1) all generated charge inside the sample contributes to the integrated current measured in the external circuit to how far it moves through the sample, i.e. if an electron moves halfway across the sample one-half electron charge will flow through the external circuit and (2) for a constantly applied bias voltage the only way current can be induced in the external circuit is by motion of charge inside the sample.

3.1.4.2   Requirements for a TOF-Experiment

From the section above one can deduce some basic conditions that must be met for a time-of-flight experiment to be feasible. In general the description of charge carrier transport used above can only be applied to insulating solids where the transit time is short compared to the dielectric relaxation time $\tau_{rel} = \varepsilon \varepsilon_0 / \sigma$ of the material. Due to the redistribution of the background charge located inside the material the dielectric relaxation causes a screen out of the injected charge. It also affects the externally applied field by redistributing the space charge in response to the applied potential and the applied field will no longer be uniform within the sample [128]. Blocking contacts are used to avoid an additional injection of charge carriers. To guarantee a uniform field during the period of carrier drift the external voltage is usually applied as a pulse right before the carrier injection.

As shown in Eq. 3.6 and 3.7 the drifting charge carriers may also perturb the externally applied electric field within the sample. Time-of-flight experiments are therefore performed in the space charge free regime, where the density of photoinjected charge carriers is low enough, so that the self-field has little influence on the external field ($F_{self} \ll F$). This is fulfilled when the integrated charge is small

compared to CV, where C is the capacitance of the specimen and V the externally applied voltage [129]. Within this limit the photocurrent scales linearly with the density of injected charge.

In principle the lower limit of a transit time t_τ that can be measured is determined only by the RC time of the electronic circuit. The overall rise time of the system has to be shorter than the time scale of the experiment. On the other hand, the drift length $\mu_d \tau_D F$ of the charge carriers has to be longer than the sample thickness L. In other words the transit time t_τ has to be shorter than the deep trapping life time τ_D, the time until the charge carriers are finally trapped in deep traps [99, 130].

Assuming that the charge induced by the laser is small compared to the CV the limitations of a reliable time-of-flight experiment can be expressed by

$$RC \ll t_\tau \ll \tau_{rel}, \tau_d \tag{3.10}$$

where the lower limit is the RC response time and the upper is determined by the dielectric relaxation τ_{rel} and the deep trapping life time τ_d.

3.1.4.3 Transit Time Evaluation

In contrast to Gaussian transport, in the case of dispersion the excess charge carrier packet spreads out to a much higher degree in a non-symmetrical way (see section 2.3.2). In addition, the absence of a long time cut-off of the transient current makes it rather complicated to define a characteristic transit time t_τ. A number of different methods have been used in the past to evaluate the transit time. This has led to different results for t_τ depending on the particular method used and therefore has to be taken into account if one wants to compare mobility results obtained and published by different groups.

This section will provide a short overview about the different methods. A more detailed review has been presented by Qi Wang et al. [131].

Transient Photocurrent Method

The "Transient Photocurrent Method" was used by a number of authors, e.g. Scharfe et al., Pai et al., Tiedje et al. and Serin et al. [76, 132, 133, 49]. Measuring the transient photocurrent as shown in Fig. 2.4, the characteristic transit time t_τ is simply defined as the "kink" in the power law.

Method of Normalized Photocurrents

For the determination of t_τ using the "Method of Normalized Photocurrents", the photocurrent transients measured at different applied fields are normalized using
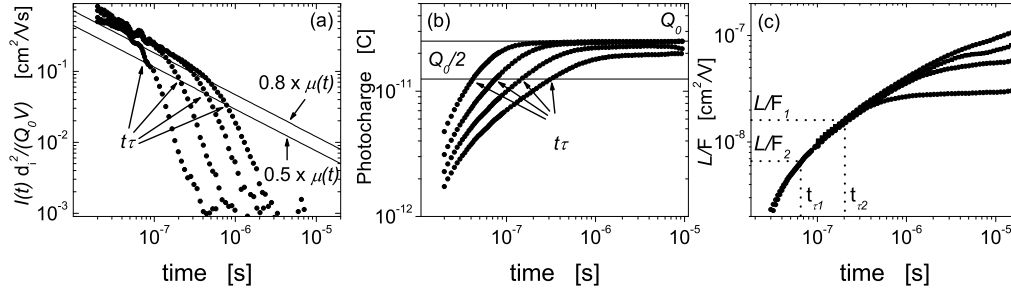
Figure 3.3: *Graphical evaluation of the transit time using the (a) method of normalized photocurrents, (b) the half-charge method, (c) the normalized photo charge technique as described in the text. Each panel shows 4 different curves taken on a µc-Si:H sample at different applied voltages V.*

$I(t)d^2/(Q_0 V)$, where d equals the specimen thickness, Q_0 is the total charge of the excess charge carrier package, and V the applied voltage. As shown in Fig. 3.3 (a) the pre-transients overlap establishing an "envelope" curve $\mu(t)$. The "envelope" curve $\mu(t)$ is used to determine the transit time. About the exact evaluation of the transit time there is still some controversy. While Marshall, Street, and Thompson defined the transit time as the crossing point of the measured transient with the curve $0.8 \times \mu(t)$ [134], Nebel et al. used $0.5 \times \mu(t)$ which gives somewhat larger values of t_τ as can be seen in Fig. 3.3 [135, 136].

Half-Charge Method

The evaluation of the transit time using the "half-charge" method is based on the same principle as used for Gaussian transport. The procedure to determine t_τ is illustrated in Fig. 3.3 (b), where the transient photocharge obtained by integrating the transient photocurrents is plotted versus the time. As the number of charge carriers in the packet is determined by the value where the charge transients show an asymptotic behavior, the transit time can be extracted by evaluating the time where half the charge has been collected. This method is typically applied to determine t_τ for Gaussian transport behavior. However, Wang et al. have shown that this evaluation is also valid in the case where transport is dispersive [131]. This method has widely been used by the Schiff group [131, 137, 138].

Normalized Photo Charge Technique

The "half-charge method" described above is based on the fact that at times before the charge carriers have reached the collecting electrode, the photocharge $Q(t)$ is proportional to the distance moved by the mean position of the photocarrier distri-

bution. This can be written as the following equation, derived from calculating the electrostatic energy dissipated by a charge Q_0 in a uniform electric field F which is $Q_0 F x(t)$. Equating this with the energy furnished by the externally applied bias voltage $Q(t)V$ one gets

$$x(t) = d\frac{Q(t)}{Q_0}. \tag{3.11}$$

From Eq. 3.9 one concludes that the transit time is solely determined by the ratio L/F. Doubling both, electric field F and distance L, the transit time remains unchanged. Generalizing the distance L to $x(t)$ Eq. 3.9 can be written as:

$$\frac{L}{F} = \frac{x(t)}{F} = Q(t)\frac{d^2}{Q_0 V} \qquad \text{for} \qquad (t \ll t_\tau) \tag{3.12}$$

Equating the transit photocharge, by integrating the photocurrent, L/F can be determined by using Eq. 3.12 and can be plotted as a function of time. These graphs are referred to as "displacibiliy plots"; a typical example is shown in figure 3.3 (c). The transit time for a chosen value of L/F can be determined directly from the graph, as indicated in the figure. As this method is simply an enhancement of the half-charge method it is clear that transit times obtained are consistent with the other methods. However, there are two advantages of using this method. First, only a handful of transients are enough to obtain a continuous curve of transit times and secondly one can obtain the displacibility for transit times shorter than would be accessible by increasing the applied voltage. This method introduced by Schiff et al. in 1993 has been used by a number of other authors [131, 139, 140, 141, 142].

3.1.4.4   Experimental Arrangement

The experimental arrangement used for time-of-flight measurements is illustrated in Fig. 3.4. The charge carriers were excited using a nitrogen laser pumped dye laser (Laser Science Inc.) with a pulse width of 3 ns. As laser dye Coumarin 500 with an emission maximum at $\lambda = 500$ nm was used, so the carrier generation took place within the first 160 nm of the illuminated side of the intrinsic layer. Stronger absorbed light was intentionally avoided to prevent back diffusion problems. The intensity of the laser was attenuated with neutral density filters until the photogenerated charge was below the $CV-$limit (see section 3.1.4.2). The repetition rate of the laser was chosen to a value low enough to avoid a build up of charge in the material. A value of 2 Hz was allowable for temperatures between $T = 300$ K and 100 K.

The specimens were mounted on the cold finger of a commercial vacuum cryostat (Oxford Instruments Model DN1754). This allowed measurements in the temperature range between $T = 77$ K and 350 K. Additionally, the cryostat acted
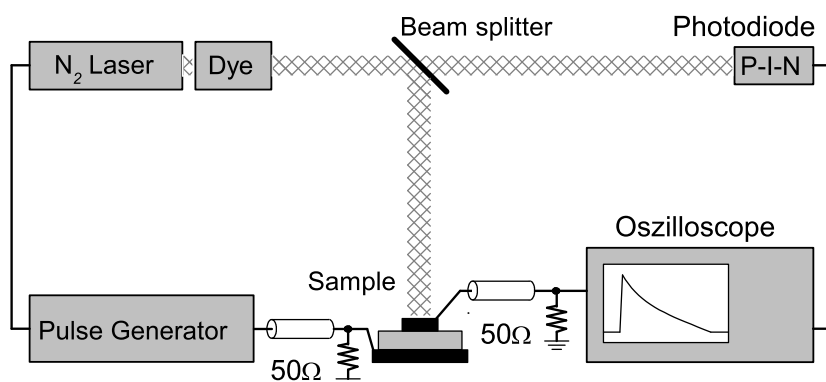
Figure 3.4: *Schematic view of the experimental setup for time of flight measurements used in this work.*

as a shield against electromagnetic interferences and also avoided influences of optical bias effects from accidental room light illumination. Great care was taken that the series resistance of the contacts was sufficiently small not to limit the time resolution of the system. To induce photocarrier drift an electric field was applied by a bias voltage across the sample. A step voltage was used to assure that the applied field was uniformly distributed (see section 3.1.4.2 and [128]). The photocurrent transients were measured by recording the voltage across a 50 Ω resistor in the time range between $t = 0 - 10\,\mu$s. For longer times a larger resistor of typical $0.3-33$ kΩ was used. In order to reduce the signal-to-noise ratio the average of 100 pulses was taken. For data acquisition and averaging of the transients a digital oscilloscope (LeCroy Model 9400, 500 MHz bandwidth) was used. The oscilloscope was connected to a computer for storage and analysis of the measured currents.

3.1.5 Thickness Measurements

In this work, thin films of μc-Si:H as well as pin diodes containing a μc-Si:H i-layer were prepared and investigated. Details of the preparation and particular structures can be found in section 3.2 and 3.3. For most of the methods presented, a knowledge of the film or the i-layer thickness is of great importance. Two different methods for thickness measurements were applied, namely mechanical step profiling and capacitance measurements. The advantages and limitations of both methods will be discussed in the following.

Mechanical measurements of the film thickness were performed using a mechanical step profiling system (Sloan DEKTAK 3030 Auto II). This method has been used for the measurements of both thin films and pin diodes. For films de-

posited on molybdenum and glass substrates the abrupt step necessary for the measurement was created by scratching the film and then applying and tearing off an adhesive tape. Thereby, a part of the film teared off from the substrate leaving a sharp edge. In the case of the pin diodes the step was created by mechanically scratching away the Si-layers using a scalpel. The bottom ZnO was then etched away with an HCl solution. Afterwards the thickness of the thin films or diodes could be measured using the mechanical step profiling system. To determine the i-layer thickness of the diodes, the thickness of the doped layers as well as the thickness of the ZnO has to be subtracted. The advantage of this method is that it measures the thickness directly with a precision of not less than 10 nm for thin films and about 50 nm in the case of the diodes. The shortcoming of this method is that an abrupt step right next to the position of interest has to be created, which especially in the case of the pin structures might destroy the device by creating shunt resistances.

Measuring the capacitance of the pin structure provides a simple, nondestructive way to determine the i-layer thickness of the PIN-diodes using:

$$C = \frac{\varepsilon \varepsilon_0 A}{d_w}.$$

(3.13)

Here ε, A, and d_w are the dielectric constant, the area of the contacts, and thickness of the depletion layer, respectively. The dielectric constant of silicon is $\varepsilon=11$. Capacitance measurements were performed using a pulse generator (Avtech, Av-1023-C) and a digital oscilloscope (LeCroy, Model 9400). Two different methods were used to estimate the capacitance. The first is to determine the RC-time constant of the sample/load resistor system, by measuring the current decay following the application of the external field on the sample. The second approach was to determine the charge induced by a voltage step. Therefore a known capacitance ($C_{ext.}$) was connected in series with the sample. As the charge between the two capacitors can only be displaced, both capacitors $C_{ext.}$ and C_{Sample} store the same amount of charge. By measuring the voltage $V_{ext.}$ across C_{ext}, the capacitance of the sample can be calculated using:

$$C_{Sample} = \frac{C_{ext.} V_{ext.}}{V_{appl.} - V_{ext.}}.$$

(3.14)

The induced charge has been measured 500 ns after the application of a voltage step. This method is commonly applied to amorphous silicon diodes and gives values which are in agreement with values obtained from physical measurements. However, it was found that for μc-Si:H structures sometimes the capacitance is up to one order of magnitude higher than calculated from the geometry of the specimen [143, 144].

3.2 Deposition Technique

Two well established and widely used techniques for the deposition of thin films of silicon are plasma enhanced chemical vapor deposition (PECVD) and hot wire chemical vapor deposition (HWCVD). Both methods are based on the decomposition of silicon containing gases. The major difference between both processes is the way how the precursors are made. While in PECVD the gases are decomposed by a plasma, in HWCVD the reaction takes place at a hot wire usually made of tungsten or tantalum. Both deposition techniques will be briefly described in the following section.

3.2.1 Plasma-Enhanced Chemical Vapor Deposition (PECVD)

A very common method for the preparation of microcrystalline silicon is plasma enhanced chemical vapor deposition (PECVD), also known as glow discharge deposition. Detailed information about this technique and the underlying physics can be found in the literature, e.g in the books by Chapman [145], Haefer [146], Frey and Kienel [147], or Luft and Tsuo [148]. In this work, a 6-chamber deposition system with designated chambers for p−, n−, and intrinsic layers was used. A detailed description of the technical realization can be found in the work by Vetterl [12].

In the PECVD process the source gases are decomposed by an electrical discharge. The main mechanism for the decomposition is the impact of electrons, that take up sufficient energy from an alternating electrical field with typical frequencies in the range between 13.56 and 150 MHz. The precursors arising diffuse and drift to the substrate, usually placed on one electrode, and contribute to the film growth after several secondary gas phase reactions. The detailed plasma chemistry and growth mechanism are of course much more complex. A major advantage of PECVD is that the activation energy for the dissociation of the source gases comes from an externally applied alternating electric field and does not need to be supplied thermally. Therefore the substrate temperature T_S can be adjusted independently, allowing the use of low T_S.

Deposition Parameters

The main source gas for the deposition of amorphous and microcrystalline silicon is silane (SiH_4). An overview about the possible reactions in a silane plasma was given by e.g. Perrin et al. [149]. The structure and the electro-optical properties of the silicon films depend on various deposition parameters. It has been shown that with the admixture of hydrogen (H_2) to the silane plasma or by the use of high discharge powers microcrystalline growth can be achieved [150]. In particular the

admixture of hydrogen (H$_2$) offers a straightforward way to change the growth conditions all the way from highly crystalline to amorphous growth. The silane concentration SC defined as the ratio of silane gas flow and the total gas flow, is therefore one of the main parameters varied in this work.

$$SC = \frac{[SiH_4]}{[SiH_4] + [H_2]} \tag{3.15}$$

Besides the gas composition several of other parameters are significant in determining the properties of the deposited films; the deposition pressure p, the substrate temperature T_S, and the plasma power density P. The plasma excitation frequency ν_{ex} is also very important for the film properties and classifies the process into RF-PECVD (standard frequency of 13.56 MHz) and VHF-PECVD (higher frequencies up to 150 MHz). Doping can be achieved by adding trimethylboron (TMB) or diborane (B$_2$H$_6$) and phosphine (PH$_3$) for p-type and n-type doping, respectively[3]. Deposition parameters used throughout this work are listed in table 3.1

Table 3.1: Typical PECVD-Deposition Parameters used within this work.

Parameter		value
Excitation frequency	ν_{ex}	95MHz (VHF)
Plasma power density	P	0.07 W/cm^2
Substrate temperature	T_{Sub}	200°C
Pressure	p	40 Pa
Silane concentration	SC	2 - 100%
Phosphor doping	PC	0 - 20 ppm
Boron doping	BC	0 - 70 ppm

3.2.2 Hot-Wire Chemical Vapor Deposition (HWCVD)

Hot-wire chemical vapor deposition (HWCVD), also known as catalytic chemical vapor deposition (CAT-CVD) [151, 152, 153], is becoming increasingly popular in the field of silicon thin film deposition, particulary since recently it was

---

[3]Doping densities are typically measured in parts per million (ppm). Taking the density of crystalline silicon a doping density of 1ppm corresponds to about 5×10^{16} doping atoms per cm^3. However, the built-in factor as well as the doping efficiency of the dopant have to be taken into account in order to determine the active doping density.

demonstrated that solar cells prepared with HWCVD can show power conversion efficiencies comparable to solar cells prepared with PECVD [13]. The use of HWCVD instead of PECVD promises higher deposition rates for μc-Si:H (30 Å/s and higher [154, 155]) and prospects for upscaling [156], which however has only partly been fulfilled so far [13].

Although the dissociation of silane is of catalytic nature, wire temperatures of $T > 1500$K are necessary for the decomposition of silane and hydrogen that are used as source gases for the film growth. The choice of material used for the wire is therefore limited by thermal stability; tantalum and tungsten are typical choices. Both materials desorb only atomic silicon and hydrogen at temperatures higher than 1700K [157]. Only at lower temperatures the dissociation into silyl radicals like SiH_2 and SiH_3 is of some importance. For a detailed discussion about the HW deposition technique, gas phase reactions, and the technical realization of these processes see [13] and references therein.

Deposition Parameters

As in PECVD, the main source gases for the deposition of amorphous and microcrystalline silicon are SiH_4 and H_2. The structure and composition of the resulting films can be varied by simply changing the hydrogen dilution. A second parameter varied in this work is the substrate temperature, which has a major influence on the properties of the deposited films. Typical hot-wire deposition parameters used throughout this work can be found in table 3.2.

Table 3.2: Typical HWCVD parameters used in this work.

Parameter		value
Filament temperature	T_F	1530°C−1650°C
Substrate temperature	T_{Sub}	180°C −450°C
Pressure	p	3.5-5 Pa
Silane concentration	SC	3 - 25 %

3.3   Sample Preparation

In this work material prepared by HWCVD as well as PECVD has been investigated. For the different experimental methods applied (see section 3.1), different substrates and structure configurations are necessary. Details of the preparation of the different samples and structures will be given in the following sections.

3.3.1 Sample Preparation for ESR and conductivity measurements

For ESR measurements the use of powdered samples allows large amounts of material to be placed in the resonant cavity. This results in high signal intensities and thereby an improved signal-to-noise ratio. Therefore, material investigated by ESR, is usually deposited on aluminum (Al) foil. For the deposition standard household foil (brand "Alio") was cleaned with 2-Propanol (99.5% purity) and wrapped around four glass substrates, each of 25×100 mm^2 size. Usually one of the substrates was equipped with one or two square holes (10×10 mm^2) in which a different substrate could be placed, e.g. roughened glass substrates for conductivity measurements. A typical arrangement of the substrates is shown in Fig. 3.5.

After deposition the chamber was flushed with argon for 5 minutes and then evacuated. To cool down, the substrate was kept in vacuum ($p \approx 10^{-9}$ mbar) for at least 3 hours. Afterwards, the material was immediately prepared for the measurement. The Al foil was etched away with a 16% HCl solution. The remaining flakes of μc-Si:H material were filtered out and thoroughly rinsed in de-ionized water. Finally the material was dried for about 24 hours at ambient ($T \approx 30°C$). The μc-Si:H powder was then inserted into quartz tubes with an inner diameter of 4 mm and a wall thickness of $d = 0.5$ mm. If the powder consisted of very loosely packed flakes, which was the case for highly crystalline films, the material was additionally crushed to obtain comparable packing densities and filling heights.
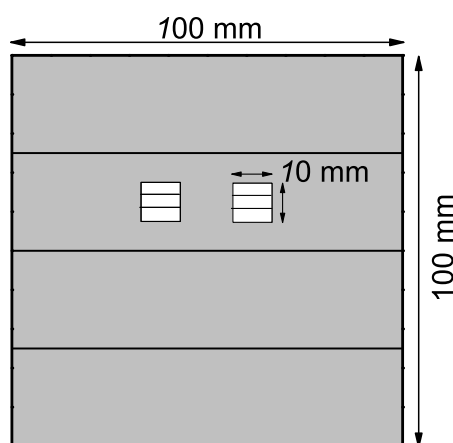

Figure 3.5: *Typical substrate arrangement for the deposition of μc-Si:H thin films using Al foil. The Al foil is wrapped around 4 glass substrates (25×100 mm^2). The square holes in one of the substrates were used to mount roughened glass substrates, which were co-deposited and later used for e.g conductivity measurements.*
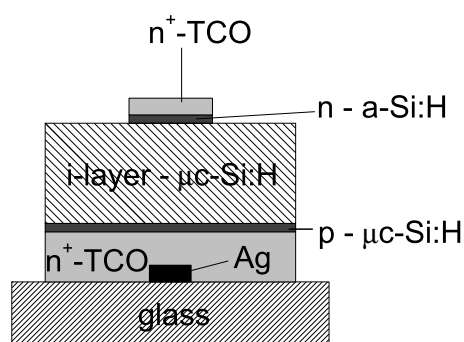
Figure 3.6: *Schematic picture of a pin diode prepared for time-of-flight measurements.*

This procedure also made sure that the material fits into the homogeneous part of the magnetic field. To maintain a defined environment, the powdered material was sealed into the quartz tubes under He atmosphere. This procedure yielded filling heights of about $0.5 - 1$ cm with a material mass between $22 - 300$ mg.

During this process the μc-Si:H is in contact with water and air for several hours. Alternatively, material has been also deposited on molybdenum foil (Mo). The foil had a size of 100×100 mm, a thickness of $d = 0.05$ mm, and a purity of 99.9%. From the Mo foil the material peeled off in flakes after bending the foil and could be sealed immediately without further treatment. As for the Al substrates, the Mo foil was equipped with a hole so that e.g. glass substrates could be deposited in the same run.

To study the influence of different environments during storing or annealing, the material was removed from the He filled tubes and sealed into Ar or O_2 atmosphere or was treated in HCl solution or water as discussed above. Samples for conductivity measurements have been prepared on roughened borosilicate glass (4×15 mm^2) in the same run as their ESR counterparts. Roughened glass was used because films with a thickness larger than $d = 1$ μm tend to peel off from a smooth substrate. After deposition, coplanar silver contacts were evaporated under high vacuum conditions having a thickness of 700 nm, a width of 4 mm, and a distance of 0.5 mm.

3.3.2   PIN-Diodes for Transient Photocurrent Measurements

Besides limitations due to the material investigated, the main criterion for a specimen suitable for time-of-flight (TOF) measurements is the existence of blocking contacts. The samples used for time-of-flight measurements were pin structures as shown in Fig. 3.6 which were prepared using VHF-PECVD (for details about the process see section 3.2.1). As in forward bias the pin diode passes the current, in

reverse bias mode the contacts do not inject charge. Another advantage of the pin structure is that it is essentially the same as used for solar cells, so the measured TOF properties can be directly related to the device performance.

Sodium-free laboratory glass (Corning 1737) was used as substrate. To contact the diode to the external circuit, silver stripes with a thickness of $d = 700$ nm and a width of $b=1$ mm were evaporated on to the glass. As transparent conductive oxide (TCO), aluminum doped zinc oxide (ZnO:Al) was deposited by rf-magnetron sputtering; for a detailed description of the process see [158]. To avoid contamination the deposition of the p, i, n layers took place in designated chambers of a PECVD system. The p-layer was prepared in the highly crystalline growth regime (SC=1.5%) with a thickness of $d = 30$ nm. Doping was achieved by adding trimethylboron (TMB - $B(CH_3)_3$) to the silane-hydrogen gas mixture. To avoid contamination of the i-chamber after deposition of the p-layer, the p-chamber was purged with argon for 5 minutes and afterwards pumped below a pressure of $p < 2 \times 10^{-8}$ mbar before the substrate was transferred. The intrinsic μc-Si:H layers were prepared using a silane-hydrogen mixture of SC=5-6%. Several diodes with varying i-layer thicknesses in the range between d=2 μm and d=6.5 μm were prepared. After the deposition of the i-layer, the chamber was again purged with argon and pumped to a pressure of $p < 2 \times 10^{-8}$ mbar before the specimen was transferred into a n-chamber and a d=30 nm n-layer was deposited on top of the structure. The n-layer was amorphous silicon a-Si:H(P) where phosphine was used as doping gas. As contacts RF-magnetron sputtered ZnO:Al dots with diameters between $1 - 2$ mm and a thicknesses of d=100 nm were used. After deposition, the top surface of these structures were plasma-etched (SF_6-gas process), in order to remove the n-layer from regions not under the ZnO:Al.

Solar cell "sister" samples were prepared in the same run as the diodes used for the TOF measurements. Here the ZnO:Al on top of the n-layer was replaced by a silver (Ag) back reflector. These structures showed lower power conversion efficiencies compared to the best solar cells obtained for this material [159]. The lower conversion efficiencies are due to a decrease in short circuit current density J_{SC} by the smooth TCO as front contact and the choice of the back-reflector.